J. Fluid Mech. (2006), *vol.* 568, *pp.* 173–192.
doi:10.1017/S0022112006002205 Printed in the United Kingdom

Axial stability of Taylor bubbles

By X. LU[1] AND A. PROSPERETTI[1,2]

[1]Department of Mechanical Engineering, The Johns Hopkins University, Baltimore, MD 21218, USA

[2]Faculty of Applied Physics, Twente Institute of Mechanics, and Burgerscentrum, University of Twente, AE 7500 Enschede, The Netherlands

(Received 17 November 2005 and in revised form 26 April 2006)

Long gas bubbles rising in a vertical tube are observed to lose axial symmetry and become unstable in a downward liquid flow. In this paper an approximate linear stability analysis of this phenomenon is presented. It is found that, under the combined effect of gravity and the pressure gradient which drives the liquid flow, the relative velocity between the bubble and the liquid decreases with increasing downflow, which diminishes the stabilizing effect of convection. The decrease of the relative velocity is accompanied by a flattening of the bubble nose, which also has a destabilizing effect by strengthening the Rayleigh–Taylor instability at the bubble nose.

1. Introduction

Slug flow in vertical tubes is characterized by large gas bubbles, often with a length of several tube diameters, separated by liquid masses – the so-called 'slugs'. When the tube diameter is not too large, the large bubbles (also known as Taylor bubbles) are smooth and glossy, with a bullet-shaped nose, and they rise at a constant velocity along the axis of the tube. The general impression is that of an axisymmetric flow endowed with a remarkable degree of stability which, on a closer consideration, cannot but appear paradoxical in view of the unstable stratification of the heavy liquid over the much lighter gas.

The same paradoxical stability is encountered with large, spherical-cap bubbles rising in an unbounded liquid. Batchelor (1987) has studied this system and has argued that the stabilization mechanism depends on a two-fold effect of the convection over the bubble surface. In the first place, as they are swept along the bubble surface, perturbations are stretched and, therefore, kinematically damped. This is a standard stabilization effect also encountered in other contexts such as curved flame fronts (see e.g. Zel'dovich *et al.* 1980), spherically growing bubbles (see e.g. Plesset 1954; Plesset & Prosperetti 1977), stretching jets (Frankel & Weihs 1987), and the so-called Bell–Plesset effect (see e.g. Epstein 2004). Secondly, there is only a finite time available for amplification before the perturbations are swept to the bubble rim. To explain the fact that, experimentally, there appears to be an upper bound to the size of spherical cap bubbles, Batchelor notes that the time available for growth increases with the radius of the bubble thus permitting some perturbations to grow so large as to destroy the integrity of the gas mass. Surface tension plays an important role in the phenomenon as, in its absence, the growth rate of the inviscid Rayleigh–Taylor instability would be proportional to the square root of the wavenumber, which would permit an arbitrarily large growth even within a short convection time.

It is likely that the same processes are relevant in explaining the fact that Taylor bubbles are not found in very large tubes. Martin (1976) quotes an unpublished

observation by Hsu & Simon of a single Taylor bubbles in water in a 300 mm diameter tube, but in his own experiments he observed a not-quite-stable bubble in a 101.6 mm diameter tube, but not in a 140 mm diameter one. In their experiments with vapour–liquid flow, Kawanishi, Hirao & Tsuge (1990) found 'no typical slug flow' in a 102.3 mm diameter vertical pipe. Batchelor's (1987) estimate of a maximum tube diameter of 460 mm is probably an upper limit that it would be difficult to achieve, except perhaps in very controlled situations.

In addition to the instability related to the tube size, Taylor bubbles exhibit another kind of instability which is of practical interest in that it has a strong effect on their rise velocity, and therefore on the gas hold-up in the slug flow regime, the period between slugs, the pressure drop, and other features. This instability arises when the bubbles rise in a counter-current liquid flow. In the words of Griffith & Wallis (1961), 'As the downward flow water velocity was increased, a point was reached at which the stable character of the bubble suddenly changes.... The nose of the bubble began to distort, to become alternately eccentric on one side or another, and to lean over to one side of the tube'. With its nose pushed to the wall, the bubble faces a slower liquid flow and is thus able to rise faster than it would otherwise. On the other hand, the bubble behaviour in an upward liquid flow is quite stable and similar to that in a quiescent liquid (Griffith & Wallis 1961; Nicklin, Wilkes & Davidson 1962; Bendiksen 1984).

The instability in downflow was first documented in some detail by Griffith & Wallis (1961) who observed it in air–water flow in tubes with diameters of 1, 3/4, and 1/2 in. (25, 19, and 13 mm, approximately). Similar observations were reported by Nicklin *et al.* (1962), Martin (1976), and Polonsky, Shemer & Barnea (1999). Martin's (1976) work dealt specifically with downward flow and documented the extreme instability of bubbles in tubes with diameters of 101.6 mm and larger. In his 26 mm diameter tube the bubbles were more stable, but under no circumstances was he able to observe stationary or downward moving axisymmetric Taylor bubbles. Other existing experimental work on downward gas–liquid flow (e.g. Spedding & Nguyen 1980; Barnea, Shoham & Taitel 1982; Mukherjee & Brill 1985; Kawanishi *et al.* 1990) is mostly concerned with flow regime transition and does not distinguish between axisymmetric and non-axisymmetric slug flow.

In the cited paper, Griffith & Wallis write: 'No satisfactory explanation or theory was formed for the bubble instability which was observed for downflow. It is also unknown as yet whether such instability could occur for upflow in very large pipes or if a reverse water flow is essential'.

In this paper we make an attempt to study the origin of this instability. The key element that emerges from our analysis is that the relative velocity between the bubble and the liquid decreases as the liquid downflow velocity increases. This circumstance leads to a decreased effectiveness of the convective stabilization mechanisms described before. The decrease of the relative velocity, accompanied by a flattening of the bubble nose, is a consequence of the competition between the gravitational pressure gradient and the imposed pressure gradient necessary to drive the fluid downward. Thus, one would conclude that the instability investigated here does require a 'reverse water flow'.

Other than the paper by Batchelor (1987), the only study dealing with the stability of three-dimensional Taylor bubbles is by Abarzhi (1998), in which the stability of bubbles rising in a quiescent liquid with various spatial periodicities is studied; although the hexagonal periodicity approximates a bubble in a round tube, the correspondence is clearly not exact. Abarzhi finds stable solutions only in a narrow

range of curvatures of the bubble nose. At the lowest order in the approximation, the fastest member of this family of solutions has a rise velocity U_B close to that given by Layzer (1955):

$$U_B = \sqrt{\frac{gD}{2k_1^0}} \simeq 0.361\sqrt{gD} \tag{1.1}$$

where $k_1^0 \simeq 3.8317$ is the first positive zero of the Bessel function J_1, g is the acceleration due to gravity, and D is the tube diameter. This result differs slightly from those given by Dumitrescu (1943) and by Davies & Taylor (1950), in which the numerical constant is 0.351 and 0.328, respectively. Dumitrescu's estimate of the Froude number $Fr = U_B/\sqrt{gD}$ is usually considered the most accurate one and agrees well with experiment (Fabre & Liné 1992).

Results such as (1.1), derived for infinitely long bubbles, are found to describe quite accurately the rise velocity in a quiescent liquid of bubbles of any length down to a couple of tube diameters (see e.g. Griffith & Wallis 1961; Nicklin *et al.* 1962), provided a Reynolds number defined as $D\sqrt{gD}/\nu$ (with ν the kinematic viscosity of the liquid) exceeds approximately 200 to 300 (see e.g. Nicklin 1962; Zukoski 1966; Fabre & Liné 1992; Viana *et al.* 2003). A correction for surface tension effects is however necessary when the Eötvös number $Eo = \rho g D^2/\sigma$ (with ρ the liquid density and σ the surface tension parameter) is smaller than a value between 40 (e.g. Tung & Parlange 1976; Bendiksen 1985; Viana *et al.* 2003) and 70 or, possibly, more (e.g White & Beardmore 1962; Zukoski 1966; Martin 1976; Nickens & Yannitell 1987). For water and normal gravity, the limitation on the Eötvös number is the more stringent of the two and corresponds to tube diameters greater than between 17 and 22 mm.

Abarzhi's study was an attempt to appeal to stability considerations to narrow down the infinity of possible solutions first found by Garabedian (1957; see also Vanden Broeck 1984*a*, *b*) for the two-dimensional problem, and later confirmed by Levine & Yang (1990) and Vanden Broeck (1991) for the three-dimensional one. There are several similarly motivated studies of the stability of two-dimensional Taylor bubbles (see e.g. Tanveer 1987; Nie & Tanveer 1995), all of which however differ from the present one in that the liquid far ahead of the bubble is at rest. The study of the stability of two-dimensional curved fronts by Bensimon, Pelce & Shraiman (1987) focuses on short-wave instabilities while that of present concern is clearly a long-wave phenomenon.

A general feature that emerges from a reading of the cited literature (as well as many other papers in this general area), is that this class of flows presents quite a number of difficulties and perplexing features (Saffman 1986; Viana *et al.* 2003; Funada *et al.* 2005). For example, Saffman (1986) writes: the mystery 'is the reason for the observed stability when the theory which predicts instability also calculates the steady shape so accurately'. The present analysis is no exception. We find our share of ambiguities but the results appear to be in reasonable consistency with experiment and a plausible explanation of the physical mechanism of the instability emerges from the analysis.

We start from an approximation derived in Collins *et al.* (1978) for the axisymmetric bubble shape in a fully developed Poiseuille liquid flow and present a linear stability analysis under the assumption that the perturbation is irrotational. This apparent inconsistency in the way in which viscous effects are accounted for was justified in Collins *et al.* (1978) whose procedure is supported further by the remark of Fabre & Liné (1992): 'viscosity acts essentially to develop the liquid velocity profile far ahead

of the bubble – but it has no influence near the front if inertia still dominates'. The same point of view is adopted, explicitly or implicitly, in a large number papers in this general area (see e.g. Dumitrescu 1943; Davies & Taylor 1950; Collins *et al.* 1978; Nickens & Yannitell 1987; Meiron 1989; Clanet, Héraud & Searéby 2004; Baumbach, Hopfinger & Cartellier 2005). (The very existence of a steadily rising bubble in a closed tube relies on the presence of viscous effects to dissipate the continuously decreasing potential energy of the gravity field. Thus, strictly speaking, a potential theory analysis of steady bubble motion is inconsistent.)

Viscosity is known to dampen surface waves over a time scale of the order of $1/(\nu k^2)$, where k is the wavenumber (see e.g. Lamb 1932). A surface disturbance originating near the axis is convected around the bubble nose in a time of the order of D/U_B, during which it will have attenuated by an amount $\nu k^2 D/U_B$. As will be seen in the following, the disturbances of present concern are only active as long as they are near the front of the bubble and have typical wavelengths of the order of D, so that viscous damping would be expected to dampen them by an amount ν/DU_B, which is of the order of the inverse Reynolds number. Thus, viscous effects may be expected to have little effect as long as the Reynolds number is sufficiently large.

In the Appendix we present a similar analysis for a base flow given by a generalization of that used by Davies & Taylor (1950). While this flow presents some artificial features, the general conclusion to which it leads is consistent with that of the more realistic Collins *et al.* base flow and, therefore, strengthens the findings of this work.

2. Theoretical framework

Since, in the unperturbed state, the bubble rises with a constant velocity, we take a frame of reference with the origin at the position of the unperturbed bubble nose and the z-axis oriented vertically upward. We use dimensionless variables in which lengths are non-dimensionalized by the tube diameter D, velocities by $\sqrt{gD}$, and pressures by $\rho g D$, with ρ the liquid density. Dimensional variables are however used in the figures and figure captions.

Neglecting viscosity, but allowing for the presence of vorticity, we write the liquid momentum equation as

$$\frac{\partial \boldsymbol{v}}{\partial t} + \nabla\left(\tfrac{1}{2}\boldsymbol{v}\cdot\boldsymbol{v} + \Pi + z\right) + \boldsymbol{\Omega}\times\boldsymbol{v} = 0, \tag{2.1}$$

where $\boldsymbol{v}$ is the velocity, $\boldsymbol{\Omega} = \nabla\times\boldsymbol{v}$ the vorticity, and Π the pressure. Upon integrating this equation along any line $\mathscr{L}$, we find

$$\int_{\mathscr{L}} \frac{\partial \boldsymbol{v}}{\partial t}\cdot \mathrm{d}\boldsymbol{x} + \tfrac{1}{2}\boldsymbol{v}\cdot\boldsymbol{v} + \Pi + z + \int_{\mathscr{L}} (\boldsymbol{\Omega}\times\boldsymbol{v})\cdot\mathrm{d}\boldsymbol{x} = C(t) \tag{2.2}$$

where $C(t)$ is an integration constant which can, in principle, depend on time.

Let now

$$\boldsymbol{v} = \boldsymbol{U} + \epsilon\boldsymbol{u}, \qquad \boldsymbol{u} = \nabla\phi, \qquad \Pi = P + \epsilon p, \tag{2.3}$$

where $\boldsymbol{U}$ and P are the steady, unperturbed velocity and pressure fields, and the perturbation velocity $\boldsymbol{u}$ is approximated as irrotational. Take the line $\mathscr{L}$ to be the trace of the unperturbed bubble on the meridian plane starting at the origin. Then, upon separating the perturbation from the base flow and using the fact that $\boldsymbol{U}$ and $\mathrm{d}\boldsymbol{x}$ are co-planar, we have

$$\tfrac{1}{2}\boldsymbol{U}\cdot\boldsymbol{U} + P + z = C_0 \tag{2.4}$$

and†

$$\frac{\partial \phi}{\partial t} + \boldsymbol{U}\cdot\boldsymbol{u} + p + \int_0 (\boldsymbol{\Omega}\times\boldsymbol{u})\cdot \mathrm{d}\boldsymbol{x} = 0. \tag{2.5}$$

Since the origin is a stagnation point for the base flow, the integration constant C_0 in the equation (2.4) must equal the pressure P_B at the origin. With the neglect of surface tension, this will also be the pressure in the bubble, which we may take as spatially uniform, neglecting hydrostatic effects in the gas. With these approximations, the liquid pressure at the interface P will also equal P_B and (2.4) simply becomes

$$\boldsymbol{U}\cdot\boldsymbol{U} = -2z. \tag{2.6}$$

In order to specify the boundary conditions, we write the unperturbed free surface as

$$S_0 \equiv r - f(z) = 0 \tag{2.7}$$

with $f(0) = 0$, while, after the perturbation,

$$S = S_0 - \epsilon h \equiv r - f(z) - \epsilon h(\theta, z, t) = 0. \tag{2.8}$$

The kinematic boundary condition

$$\left[\frac{\partial S}{\partial t} + \boldsymbol{v}\cdot\nabla S\right]_{S=0} = 0 \tag{2.9}$$

separates into the two relations

$$[\boldsymbol{U}\cdot\nabla S_0]_{S_0=0} = 0, \tag{2.10}$$

and

$$u_r - f' u_z = \frac{\partial h}{\partial t} - h\frac{\partial}{\partial r}(U_r - f' U_z) + U_z \frac{\partial h}{\partial z} \tag{2.11}$$

where indices denote components.

With the neglect of surface tension, the dynamic boundary condition is

$$[P + \epsilon p]_{S=0} = P_B \tag{2.12}$$

which gives, for the perturbation

$$\left[h\frac{\partial P}{\partial r} + p\right]_{r=f} = 0. \tag{2.13}$$

Since $\partial P/\partial r$ vanishes for $r = 0$, so does p. As a consequence, (2.5) shows that $\partial\phi/\partial t = 0$ at the nose of the unperturbed bubble.

It can be shown that, near the bubble nose, the perturbation equations (2.5) and (2.11) (the latter without the vorticity contribution) coincide with Batchelor's (1987) formulation.

3. The base flow

Collins *et al.* (1978) presented a solution for the rise of a Taylor bubble in a viscous liquid by approximating the flow as inviscid, but retaining in the incident flow the

† If one were to write $C(t) = C_0 + \epsilon c(t)$, the right-hand side of (2.5) would be $c(t)$ rather than 0. However, since c is only a function of time, it can be absorbed in a redefinition of the potential, $\phi \to \phi + \int c(t)\,\mathrm{d}t$ which leaves the perturbation velocity unchanged.

same vorticity that would be generated by viscous stresses. We base our analysis on their model A, the simpler of the two models that they use for laminar incident flow.

In this model only one term of an infinite series expansion for the stream function Ψ is retained:

$$\Psi = \tfrac{1}{2}U_B r^2 - \overline{U} r^2(1-2r^2) + (U_B - 2\overline{U})\frac{r}{2k_1^0}\exp\left(-2k_1^0 z\right)J_0'\left(2k_1^0 r\right). \tag{3.1}$$

Here $\overline{U}$ is the average velocity in the tube made dimensionless by division by $\sqrt{gD}$; positive and negative $\overline{U}$ correspond to upward and downward liquid flow, respectively. The incident velocity distribution is parabolic, oriented in the opposite direction to the flow. The vorticity is given by

$$\boldsymbol{\Omega} = \boldsymbol{e}_\theta(\partial_z U_r - \partial_r U_z) = 16\overline{U} r \boldsymbol{e}_\theta \tag{3.2}$$

in which $\boldsymbol{e}_\theta$ is a unit vector in the angular direction. The surface $\Psi = 0$ is the bubble surface:

$$Z(r) = -\frac{1}{2k_1^0}\log\left[\frac{k_1^0 r}{J_1(2k_1^0 r)}\left(1 + \frac{4\overline{U} r^2}{U_B - 2\overline{U}}\right)\right]. \tag{3.3}$$

The dashed lines in figure 1 show the bubble shape corresponding to $\overline{U} = 0.1$, 0, -0.1, and -0.2; the solid lines will be explained later in § 6. It can be seen here that, as the upward liquid velocity is gradually decreased and becomes negative, the bubble becomes flatter and flatter, with the radius of curvature at the nose increasing from $2/k_1^0 \simeq 0.522$ for $\overline{U} = 0$ (the experimental value is closer to 0.350, Fabre & Liné 1992, or 0.375, Funada *et al.* 2005), to $6/k_1^0 \simeq 1.567$ for the limit value $\overline{U} \simeq -0.255$ (see below). This trend can be understood by noting that the liquid flow requires the action of a pressure gradient which combines with gravity to drive the bubble motion. For upward liquid flow the effect of the imposed gradient is in the same direction as that of gravity, while it is in the opposite direction for downward liquid flow. As a consequence, as will be shown presently, the velocity of the bubble relative to the liquid will be greater in upflow than in downflow. Because of the obstruction caused by the bubble, the liquid must accelerate but since, along the bubble, it is essentially in free fall (see e.g. Nicklin *et al.* 1962), this acceleration can only be obtained at the expense of gravitational potential energy. This circumstance limits the rate at which the bubble cross-section can grow with the consequence that the higher the relative velocity the more tapered (i.e. more pointed) is bubble. The mechanism by which the bubble shape is adjusted in this way is the dynamic pressure: a higher relative velocity means a larger dynamic pressure, which will push the bubble surface further down.

Upon substitution of the expressions for U_r and U_z obtained from the stream function (3.1) into the dynamic condition (2.6), one finds a relation from which the bubble rise velocity U_B can in principle be determined. However, since (3.1) is only an approximation to the stream function, it is found that (2.6) cannot be satisfied for all values of r with a single U_B. Rather, the equation can only be satisfied at one point. By taking this point to be the origin, we find

$$(U_B - 2\overline{U})^2 = \frac{2}{k_1^0}\left[\frac{1}{(k_1^0)^2}\frac{2\overline{U}}{U_B - 2\overline{U}} + \frac{1}{4}\right]. \tag{3.4}$$

In particular, for a bubble rising in a quiescent liquid, $\overline{U} = 0$ and this relation gives the result quoted earlier in (1.1), $U_B = (2k_1^0)^{-1/2} \simeq 0.361$, which differs by 3% from the accepted value 0.351. In order to determine the physical root of (3.4), we follow the

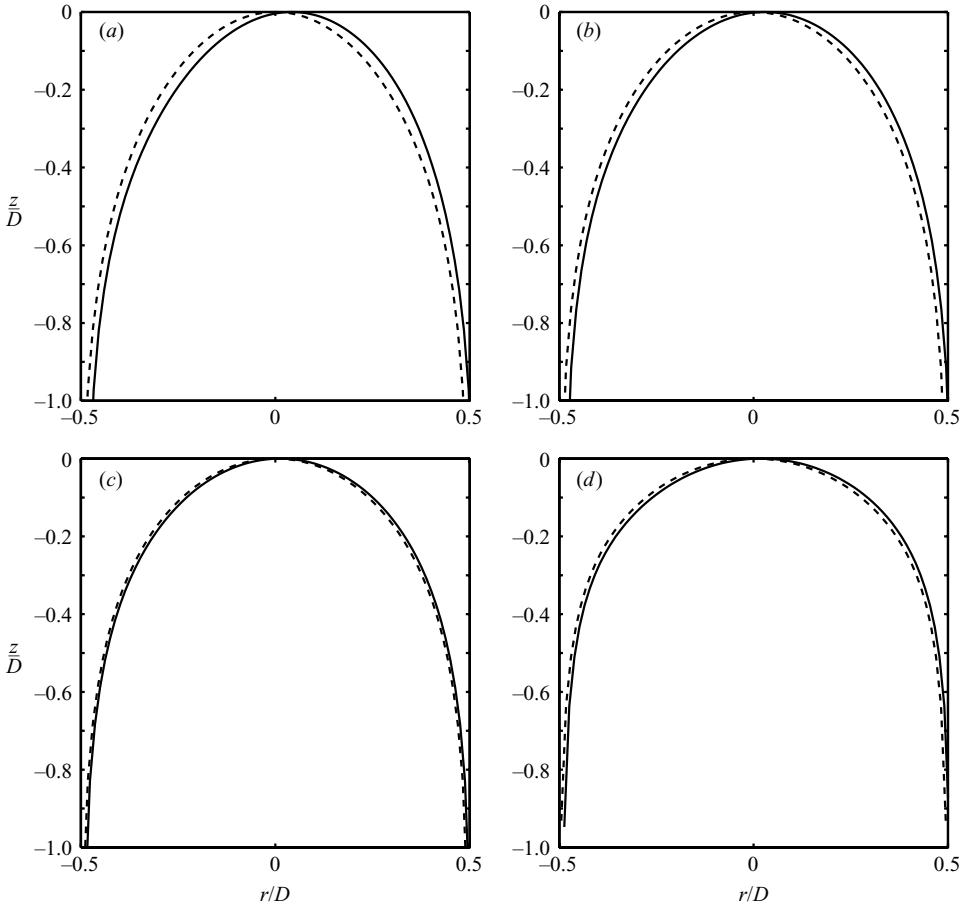

FIGURE 1. The dashed lines are the unperturbed bubble shapes for (*a*) $\overline{U}/\sqrt{gD} = 0.1$, (*b*) 0, (*c*) −0.1, (*d*) −0.2 (left to right, top to bottom). The bubble becomes more and more blunt as the velocity is decreased. The solid lines are the perturbed shapes as described in § 6.

branch to which this root belongs with decreasing $\overline{U}$. This root becomes complex for $\overline{U} = -\frac{1}{2}(k_1^0/6)^{3/2} \simeq -0.255$, which corresponds to $U_B = [1-(k_1^0)^2/6]\sqrt{1/(6k_1^0)} \simeq -0.301$. This root is always greater than the liquid velocity on the tube axis, $2\overline{U}$, and always greater than $\overline{U}$ except in a small region near $\overline{U} = -0.244$. Whenever there is more than one root, this root is larger than the others, thus satisfying Garabedian's (1957) criterion for stable equilibrium. The bubble starts moving downward for $U_B = 0$ which corresponds to $\overline{U} = -\frac{1}{2}\sqrt{(1-4/(k_1^0)^2)/2k_1^0} \simeq -0.154$. The relation between U_B and $\overline{U}$ given by (3.4) is shown by the solid line in figure 2(*a*).

The dashed line in figure 2(b) shows the dependence of the bubble rise velocity on $\overline{U}$ if (2.6) is evaluated at $r = 1/4$ rather than 0 as in Davies & Taylor (1950). While there are some differences, the results of the two evaluations are reasonably consistent. For upward liquid flow, Collins *et al.* (1978) give the approximation

$$U_B = c_1\overline{U} + c_2 \tag{3.5}$$

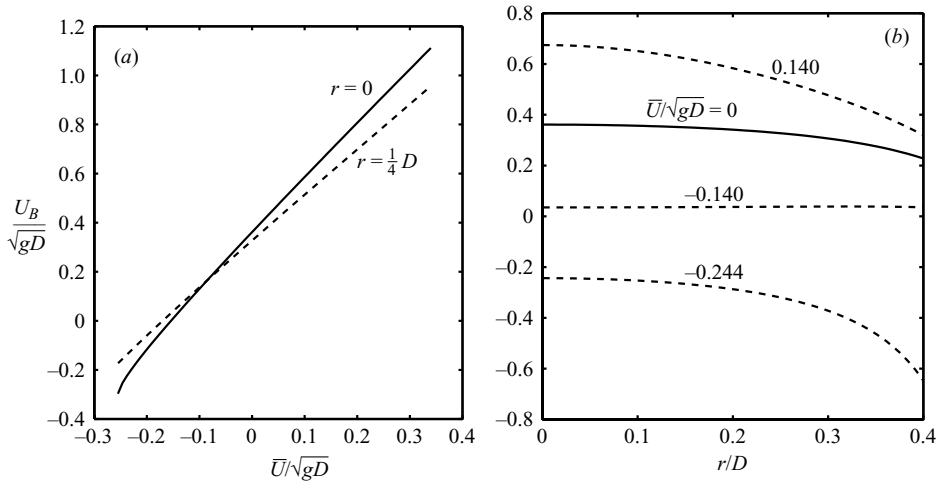

FIGURE 2. (*a*) Bubble rising velocity vs. $\overline{U}$, the mean liquid velocity in the pipe (positive upward), as calculated from (3.4). (*b*) Bubble rising velocity as calculated from (2.6) evaluated at different values of the radial coordinate r.

with $c_1 = 2.27$ and $c_2 = 0.361$. Between $\overline{U} = 0$ and 0.3, our result for the evaluation at $r = 0$ can be approximated by taking $c_1 = 2.213$ and $c_2 = 0.361$, and that for the evaluation at $r = 1/4$ by taking $c_1 = 1.86$ and $c_2 = 0.327$. This second value of c_1 is definitely too low to match experiment, which suggests that (3.4) is fairly accurate.

Figure 2(*b*) shows, for representative positive and negative values of $\overline{U}$, the predicted rise velocity U_B evaluated corresponding to different values of r. It can be seen here that, for downward liquid flows, which is the situation that interests us most in this paper, the calculated bubble rise velocity is only weakly dependent on r for r up to about 0.2. For larger values of r, however, the r-dependence increases.

4. Perturbation

Since the base flow is axisymmetric, the perturbation can be expanded on a basis of eigenfunctions of the angular variable which, by linearity, can be considered one by one. Thus, we consider an irrotational perturbation corresponding to the mth angular mode characterized by a potential given by

$$\phi \;=\; \exp(\mathrm{i}m\theta)\;\sum_{j=1}^{\infty}\alpha_j(t)\exp\left(-2k_j^m z\right)\,J_m\left(2k_j^m r\right), \tag{4.1}$$

where the α_j are functions of time to be determined. Choosing the k_j^m as the jth positive zero of J_m' satisfies the kinematic boundary condition on the tube wall. Upon substitution into the integral term of (2.5), we find

$$\int_0(\boldsymbol{\Omega}\times\boldsymbol{u})\cdot\mathrm{d}\boldsymbol{r} \;=\; 32\overline{U}\exp(\mathrm{i}m\theta)\sum_{j=1}^{\infty}\alpha_j k_j^m\int_0\exp\left[-2k_j^m Z(r)\right]\,\left[J_m + J_m' Z'(r)\right] r\,\mathrm{d}r. \tag{4.2}$$

The surface deformation is taken in the form

$$h \;=\; \exp(\mathrm{i}m\theta)\;\sum_{j=1}^{\infty}\beta_j(t)\frac{J_m\left(2k_j^m r\right)}{r} \tag{4.3}$$

with the β_j other functions of time to be determined.

The choice $m=0$ amounts to a correction of the unperturbed bubble shape and base flow and, as argued in the next section, is not particularly significant. A value of m equal to 2 would correspond to the bubble cross-section acquiring an elliptical shape, $m=3$ to a perturbation with three lobes in the angular direction, and so forth. The most interesting case for the present purposes is $m=1$ which, to lowest order, corresponds to displacing the centre of each cross-section $z=$ const. away from the axis of symmetry.

With these expressions, after truncating the infinite series to N terms, the dynamic boundary condition (2.5) becomes

$$\sum_{j=1}^{N}\dot{\alpha}_j\exp\left(-2k_j^mZ\right)J_m+\frac{1}{r}\left[(\boldsymbol{U}\cdot\nabla)U_r\right]\sum_{j=1}^{N}\beta_jJ_m$$
$$+\sum_{j=1}^{N}\alpha_j\left[2\exp\left(-2k_j^mZ\right)k_j^m\left(J_m'U_r-J_mU_Z\right)\right.$$
$$\left.+32\overline{U}k_j^m\int\exp\left(-2k_j^mZ\right)\left(J_m+J_m'Z'\right)r\,\mathrm{d}r\right]=0 \tag{4.4}$$

where dots denote time differentiation. The kinematic boundary condition is

$$\sum_{j=1}^{N}\dot{\beta}_jJ_m+\sum_{j=1}^{N}\beta_j\left[-\frac{\partial}{\partial r}(U_r-U_z/Z')J_m+U_r\left(2J_m'k_j^m-J_m/r\right)\right]$$
$$-\sum_{j=1}^{N}2\alpha_j\exp\left(-2k_j^mZ\right)k_j^mr\left(J_m'+J_m/Z'\right)=0. \tag{4.5}$$

The previous equations cannot be applied at $r=0$ as they stand. The limit is however readily calculated analytically, with the result

$$\sum_{j=1}^{N}\dot{\alpha}_j\left(k_j^m\right)^m+(U_B-2\overline{U})k_1^0m\sum_{j=1}^{N}\alpha_j\left(k_j^m\right)^m+\left[k_1^0(U_B-2\overline{U})\right]^2\sum_{j=1}^{N}\beta_j\left(k_j^m\right)^m=0, \tag{4.6}$$

$$\sum_{j=1}^{N}\dot{\beta}_j\left(k_j^m\right)^m+(U_B-2\overline{U})k_1^0(m+2)\sum_{j=1}^{N}\beta_j\left(k_j^m\right)^m$$
$$-\sum_{j=1}^{N}\alpha_j(k_j^m)^m\left[m-\frac{k_j^m}{k_1^0}\frac{1}{\left(k_1^0\right)^2\overline{2U}/(U_B-2\overline{U})+\frac{1}{4}}\right]=0. \tag{4.7}$$

The plan of the calculation is to solve the problem by collocation imposing that (4.4) and (4.5) be satisfied for N different values of r.

5. Approximation near the bubble nose

The simplest approximation is to impose the kinematic and dynamic boundary conditions at the single point $r=0$. Upon retaining only the first term of (4.6) and (4.7), and using (3.4), we find

$$\dot{\alpha}_1+(U_B-2\overline{U})k_1^0m\alpha_1+\left[k_1^0(U_B-2\overline{U})\right]^2\beta_1=0, \tag{5.1}$$

$$\dot{\beta}_1 + (U_B - 2\overline{U})k_1^0(m+2)\beta_1 - \alpha_1\left[m - \frac{2k_1^m}{\left(k_1^0\right)^2(U_B - 2\overline{U})^2}\right] = 0. \tag{5.2}$$

This is a linear system of the form $\boldsymbol{A}\dot{\boldsymbol{X}} = \boldsymbol{B}\boldsymbol{X}$, in which $\boldsymbol{A}$ and $\boldsymbol{B}$ are constant matrices and $\boldsymbol{X}^T = (\alpha_1, \beta_1)$. The solutions are proportional to $\exp(\lambda t)$ with λ given by $\det(\boldsymbol{A}\lambda - \boldsymbol{B}) = 0$. A simple calculation gives

$$\lambda = k_1^0(U_B - 2\overline{U})\left[-(m+1) \pm \sqrt{1 - m + \frac{2k_1^m}{\left(k_1^0\right)^2(U_B - 2\overline{U})^2}}\right]. \tag{5.3}$$

It is evident that a positive root always exists for an axisymmetric disturbance with $m = 0$. This class of perturbations corresponds to an adjustment of the unperturbed state and the instability is due to the fact that the bubble shape and base flow which we use are not exact. In other words, if one were to do an 'exact' axisymmetric numerical calculation starting with our assumed base flow and bubble shape, one would find an evolution of the flow and bubble shape away from the initial condition toward the exact solution. In a stability context, this evolution away from the initial condition would appear as an instability of the assumed base flow. This situation is encountered in other problems as well (see e.g. Meiron 1989): the instability is clearly spurious and can be disregarded.† Obviously, this is possible only because, in this linear study, modes with different m decouple. In a fully nonlinear analysis, the approximate nature of the base state would eventually contaminate all the modes.

For non-zero values of m since, as noted before, $U_B - 2\overline{U}$ is always positive, the stability condition $\lambda \leqslant 0$ is that the square root be smaller than $m + 1$, which gives

$$U_B - 2\overline{U} \geqslant \frac{1}{k_1^0}\sqrt{\frac{2k_1^m}{m(m+3)}}. \tag{5.4}$$

The eigenvalues given by (5.3) are shown as functions of $\overline{U}$ for $m = 1, 2$, and 3 in figure 3(a) in the physical range $\overline{U} \geqslant -0.255$. It is seen here that $m = 1$ is the least stable mode, which becomes unstable at $\overline{U} \simeq -0.239$. All other modes are stable.

6. A better approximation

The result (5.3) can be improved by imposing that (4.4) and (4.5) be satisfied for other r values in addition to $r = 0$. This procedure leads to a linear system of the same form as before, $\boldsymbol{A}\dot{\boldsymbol{X}} = \boldsymbol{B}\boldsymbol{X}$, again having exponential solutions with the eigenvalues given by $\det(\boldsymbol{A}\lambda - \boldsymbol{B}) = 0$. The only difference is that there are now $2N$ eigenvalues for the $2N$-equations system, and that $\boldsymbol{X}^T = (\alpha_1, \alpha_2, \ldots, \alpha_N, \beta_1, \beta_2, \ldots, \beta_N)$. The U_B present in (4.4) and (4.5) was evaluated from (3.4).

We take N equispaced values of r in the range $0 \leqslant r \leqslant r_{max}$. The least stable eigenvalue for $m = 1, 2$, and 3 calculated with $N = 5$ and $r_{max} = 0.35$ is shown as a function of $\overline{U}$ in figure 3(b). While the general trend of the curves is similar to that found by only considering the point $r = 0$, there are important quantitative differences.

† For example, Meiron (1989) states 'if the stability analysis ... is performed with respect to an inconsistent equilibrium solution ... then a spurious growth rate ... will be obtained' (p. 110). This comment was in connection with the claim by Hartunian & Sears (1957) to have found an 'explanation' for the deviation of a rising bubble from a rectilinear path. These authors failed to realize that their result was due to the assumption of an approximate, rather than exact, base state. As shown by Meiron, when an exact base state is assumed, the instability disappears.

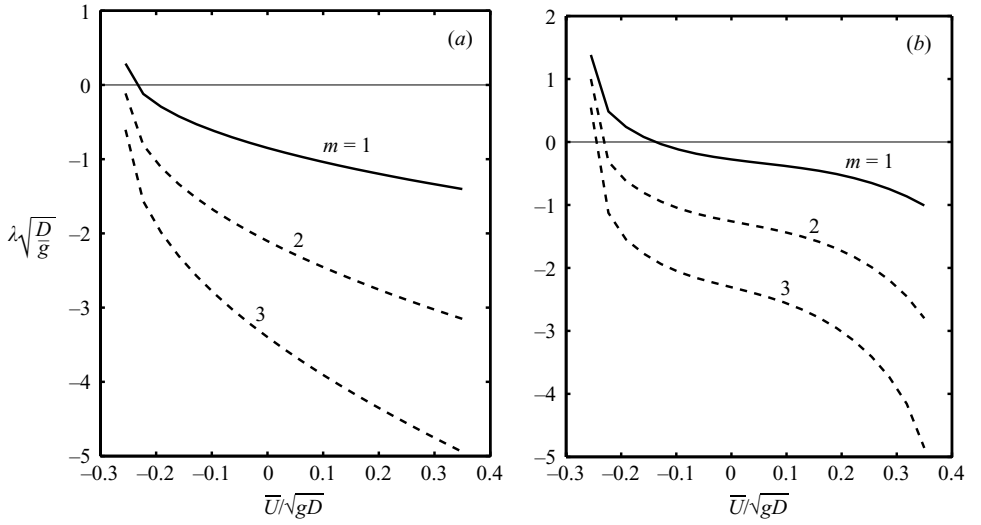

FIGURE 3. (*a*) The largest eigenvalue as calculated from the near-nose relation (5.3) vs. the liquid mean velocity for $m = 1$, 2, and 3. The mode $m = 1$ is unstable for $\overline{U}/\sqrt{gD} < -0.239$. (*b*) The largest eigenvalue as calculated from (4.4) and (4.5) evaluated at 5 equispaced points between $r = 0$ and $r/D = 0.35$ vs. the liquid mean velocity for $m = 1$, 2, and 3. The modes $m = 1, 2$, and 3 are unstable for $\overline{U}/\sqrt{gD} < -0.138$, -0.238, and -0.249, respectively

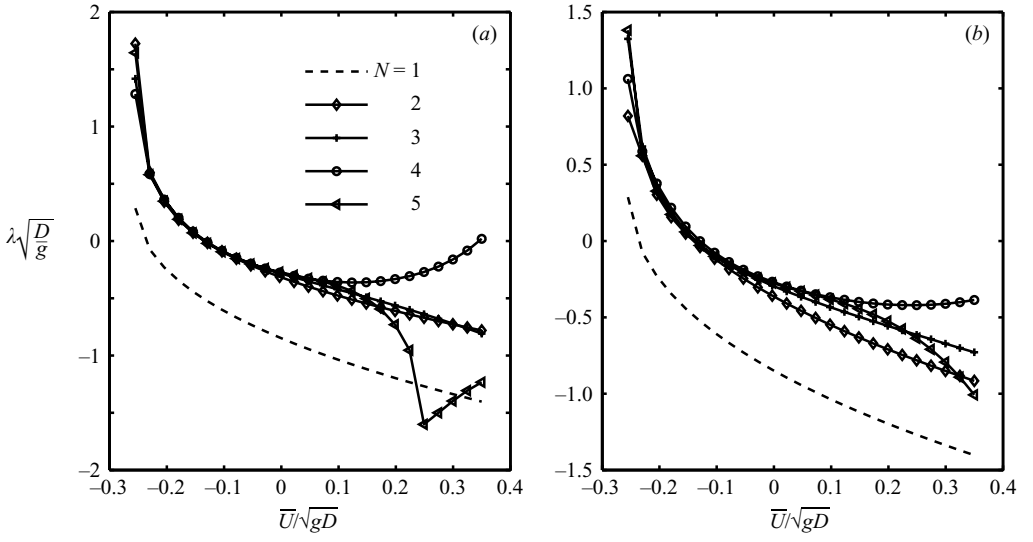

FIGURE 4. The $m = 1$ eigenvalue with the largest real part for N equispaced points between $r = 0$ and $r/D = 0.30$ (*a*) and $r = 0.35$ (*b*). The lines for $N = 1$ (dashed), are the same as shown in the figure 3(*a*).

The $m = 1$ mode becomes unstable for $\overline{U} = -0.138$ and, in addition, modes with a larger value of m are found to become unstable: that for $m = 2$ for $\overline{U} < -0.238$, and that for $m = 3$ for $\overline{U} < -0.249$.

To explore the sensitivity of the results to N and r_{max} we show in figure 4 the least stable eigenvalue for $m = 1$ for $r_{max} = 0.30$ (panel *a*) and 0.35 as a function of $\overline{U}$. The

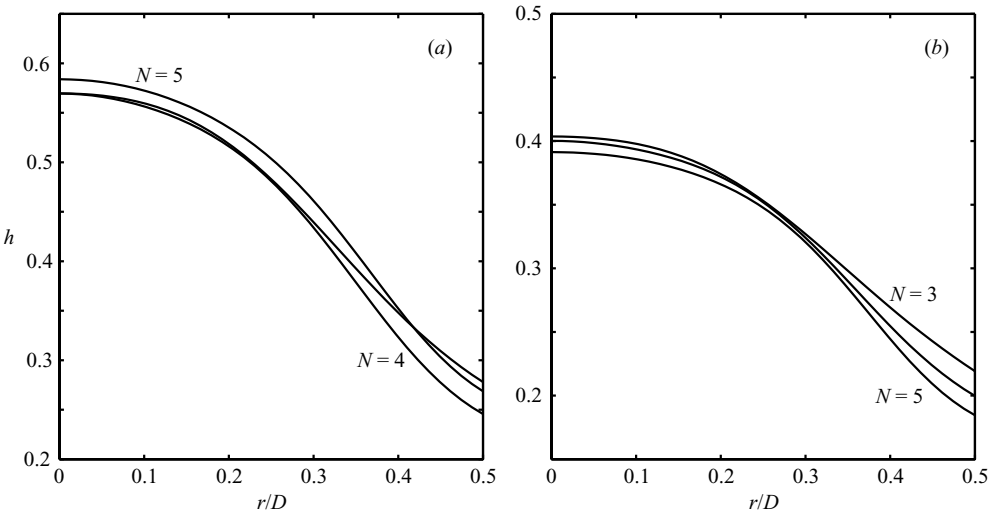

FIGURE 5. Free-surface perturbation for a stable case, $\overline{U}=0$ (a), and an unstable case, $\overline{U}/\sqrt{gD}=-0.2$ (b) as calculated for $N=3$, 4, and 5. The unlabelled curves are for $N=3$ in (a) and $N=4$ in (b).

different lines correspond to different values of N between 1 and 5. Aside from the line for $N=1$ (dashed), which in both figures is the same as that shown in figure 3(a), the various N values all predict the onset of instability for $\overline{U}$ between -0.14 and -0.13. The agreement among the results for different N is better for $r_{max}=0.30$ than for 0.35, which is probably the result of the progressive deterioration of the accuracy of the base flow as r is increased. The eigenvalue is real in most of the range shown. An exception is the case $N=5$ in figure 4(a), where the kink in the curve at about $\overline{U}=0.24$ corresponds to the transition from real to complex values. The robustness of this result is discussed further in the next section.

The predicted shape of the free-surface perturbation for $m=1$ is shown for $\overline{U}=0$ and -0.2 and $N=3$, 4, and 5 in figure 5. There is a general agreement among the predictions for different N, which deteriorates somewhat with increasing $\overline{U}$. The bubble shapes including the perturbation (multiplied by an arbitrary small number) are shown by the solid lines in figure 1, where the displacement away from the axis of symmetry of the $m=1$ mode is evident.

7. Discussion

Griffith & Wallis (1961) measured the instability threshold in downflow of 10 °C water ($\mu=1.3\times10^{-3}$ kg m^{-1}, $\nu=1.3\times10^{-6}$ m^2 s^{-1}). They used pipes of diameter 1, 3/4, and 1/2 in. (25, 19, and 13 mm). The measured thresholds can be read off their figure 3 and are, approximately, -0.11, -0.18, and -0.51 ft s^{-1} (-33.6, -54.9, and -156 mm s^{-1}), which correspond to Reynolds numbers $D\overline{U}/\nu=646$, 802, and 1560 respectively, indicating an essentially laminar flow. Upon conversion to dimensionless values by division by $\sqrt{Dg}$, these thresholds become $\overline{U}=-0.067$, -0.13, and -0.44. There is no doubt as to the importance of surface tension effects for the smallest tube, for which the Eötvös number $Eo=23$, while, for the largest tube for which $Eo=90$, surface tension may be expected to be much less important. While, as noted before, most of the existing literature places the upper limit for significant surface tension

effects at values of Eo between 40 and 70, a recent computational study (Ha-Ngoc & Fabre 2004) finds a 5% difference in the bubble rise velocity as Eo is increased from 100 to 1000. The 3/4 in. tube, with $Eo = 51$, probably falls in a transition region, although the factor 2 difference between the measured thresholds for the 1 and 3/4 in. tubes is surprisingly large and may indicate some problem with the data. The stability threshold value calculated in the previous section was between -0.14 and -0.13, which is close to the data for the 3/4 in. tube but much more negative than for the 1 in. tube. While, as just pointed out, there appear to be some uncertainties in the data, it would not be surprising if our very simple model exhibited a relatively large quantitative error. In addition to the many approximations made, in principle, enlarging the class of admitted perturbations beyond the irrotational ones might conceivably expand the unstable range.

In a short note, Nigmatulin (2001) shows a stable axisymmetric Taylor bubble rendered stationary in the laboratory frame by a downward liquid flow. As mentioned in § 3, according to our model this would happen for $\overline{U} = -0.154$ which is past the instability threshold. However these experiments were conducted in water in a 15.6 mm diameter tube, which corresponds to $Eo \simeq 33$, too small to ignore surface tension.

In spite of its quantitative uncertainty, the model sheds some light on the physical processes underlying the observed instability of the axially symmetric flow. As mentioned in § 3, as the imposed fluid velocity decreases, the relative velocity between the bubble and the liquid also decreases. This fact has two important consequences. In the first place, it decreases the stabilizing effect of convection described by Batchelor (1987) and summarized in § 1: the perturbations have more time to grow and they are stretched at a slower rate. A measure of the magnitude of this latter effect can be obtained by considering $\partial U_r/\partial r$ at the bubble nose, which is

$$\left.\frac{\partial U_r}{\partial r}\right|_{0,0} = k_1^0(U_B - 2\overline{U}). \tag{7.1}$$

Since $c_1 > 2$, the approximation (3.5) shows that this is an increasing function of $\overline{U}$, which quantifies the increasing degree of surface stretching as $\overline{U}$ is increased.

The second point is that the bubble becomes flatter so that the interface more closely approaches the situation prevailing in the standard Rayleigh–Taylor instability. In particular, the gravity component normal to the interface, which drives the instability, is larger. Heuristically, one may define an effective gravity acceleration as

$$g_{eff} = -\frac{1}{S}\int_S \boldsymbol{g}\cdot\boldsymbol{n}\,\mathrm{d}S \tag{7.2}$$

where $\boldsymbol{n}$ is the unit outward normal and the integral is extended over the portion S of the bubble surface where the acceleration due to gravity is locally directed into the gas phase. With a representation of the surface as in (2.7), a simple calculation shows that

$$\frac{g_{eff}}{g} = \frac{\displaystyle\int_0^Z \mathrm{d}z\, f'(z)}{\displaystyle\int_0^Z \mathrm{d}z\,\sqrt{1+f'^2}} = \frac{f(Z)}{\displaystyle\int_0^Z \mathrm{d}z\,\sqrt{1+f'^2}} \tag{7.3}$$

where Z is the lower boundary of the portion S of the bubble surface. For a nearly flat bubble, f' is very large and $g_{eff} \simeq g$. With increasing upward flow, the radius of curvature decreases and so does f', which leads to a decrease of g_{eff}. For example, for

a spherical bubble nose with a radius equal to the tube radius and $Z = 1/2$, a simple calculation gives $g_{eff}/g = 2/\pi \simeq 0.64$.

Retaining only the first few terms in the expansions (4.1) and (4.3) permits us only to analyse the stability of perturbations with a length scale comparable to the tube diameter. This is the reason why our results fail to capture the intermediate-wave instability that prevents the existence of axisymmetric Taylor bubbles in very large tubes. As for short waves, the neglect of surface tension deprives our results of an essential stabilizing effect at the small scales. Unfortunately, as shown by Tung & Parlange (1976) and Bendiksen (1985), the inclusion of surface tension in a model resting on the one-term representation (3.1) of the base state leads to a prediction of the dependence on the rising velocity of the Eötvös number which is not only quantitatively but even qualitatively incorrect. A stability analysis including surface tension effects would therefore be considerably more involved.

If we increase the number of terms retained, we find that spurious eigenvalues arise which are clearly unphysical as, for example, they would predict an instability of bubbles rising in a quiescent fluid for $N > 7$. Upon a close examination of the results, it is found that the surface perturbations corresponding to these spurious modes acquire more and more structure near the tube wall, which is the region where our model is least accurate. In spite of this convergence failure, we believe that our results are acceptably accurate as, in the range of r_{max} and N used to obtain them, we encounter a relative insensitivity to these parameters. Furthermore, this is precisely the range where the structure of the solution is mostly localized near the axis of the tube, which is the region directly involved in the instability and where we expect our model to be most reliable.

In addition to surface tension, viscous effects have also been neglected in our work. Other than for a stabilizing effect on the short waves, the most serious consequence of this approximation is probably the restriction to irrotational perturbations. Narrowing the class of admitted perturbations can evidently lead to an over–estimation of the stability properties of the flow, but also to the omission of other instability mechanisms dependent on vorticity. For such other effects to qualitatively change our conclusions, however, they should be sufficiently strong to overpower the Rayleigh–Taylor instability. In general, the most powerful instabilities in high-Reynolds-number fluid mechanics are those which exist also in the inviscid theory. Hence, we would expect the likelihood of other mechanisms being more important than the ones we account for to be small.

8. Conclusion

We have studied a simple model of Taylor bubbles in co-current and counter-current liquid flow in an attempt to understand the instability encountered in experiments in which the bubble rises against an incoming liquid stream. We have found that the major factor underlying the observed instability is the flattening of the bubble nose as the liquid flows downward. This effect is the result of the negative combination of gravity and the imposed pressure gradient, which results in a decrease of the relative velocity between the bubble and the liquid.

Our analysis has been conducted using a simplified model in which the bubble shape is approximated rather crudely and the perturbation is assumed to be irrotational. As a consequence, our results match experiment only in a general way, but they have proven useful in understanding the nature of the instability which is described in detail in § 7.

On the basis of our understanding of this instability, it would seem that its mechanism is generic. To illustrate this point we present in the Appendix the analysis of the stability of another base flow which, though different from the one studied here, leads to a similarly unstable situation. An interesting finding of this analysis is that the instability is only due to the deformation of the bubble nose, as the cross-section-averaged velocity of the base flow vanishes. This is yet another indication of the crucial importance of the near-axis region in the dynamics of Taylor bubbles.

In closing, it should be mentioned that Griffith & Wallis (1961) report that, after the onset of the instability, 'as downflow water velocity was further increased, the unsymmetrical shape became dominant and the motion became steady again'. It is worth noting that the possibility of such steady unsymmetrical bubbles has also been noted in two-dimensional viscous fingering in Hele-Shaw cells and porous media (Taylor & Saffman 1959). In this case one finds a two-parameter family of solutions, rather than a one-parameter family as in the symmetric case. The physical explanation of the instability studied in this paper would suggest that a similar instability would also be found in the two-dimensional case.

This study has been supported by NASA under grant NNC05GA47G.

Appendix. Potential base flow

In order to illustrate the generic nature of the instability that we have studied, it is of some interest to consider a different base flow, even if perhaps less realistic than the one studied before. In this case as well we find that the instability is associated with a flattening of the bubble nose and a decreased degree of stretching of the flow in its neighbourhood.

A.1. *Unperturbed problem*

We take the base flow to be given in terms of a potential which generalizes the form used by Davies & Taylor (1950):

$$\Phi = U_B \Phi^0 + W \Phi^1 \tag{A 1}$$

in which

$$\Phi^0 = -\left[z + \frac{1}{2k_1^0} \exp\left(-2k_1^0 z\right) J_0\left(2k_1^0 r\right)\right] \tag{A 2}$$

is the original Davies & Taylor potential, corresponding to stagnant liquid ahead of the bubble, while

$$\Phi^1 = \frac{1}{2k_1^0} \cosh\left(2k_1^0 z\right)\, J_0\left(2k_1^0 r\right) \tag{A 3}$$

is a new term. The corresponding stream function is

$$\Psi = U_B \Psi^0 + W \Psi^1 \tag{A 4}$$

with

$$\Psi^0 = \frac{1}{2} r^2 + \frac{r}{2k_1^0} \exp\left(-2k_1^0 z\right) J_0'\left(2k_1^0 r\right), \tag{A 5}$$

$$\Psi^1 = \frac{r}{2k_1^0}\, \sinh\left(2k_1^0 z\right) J_0'\left(2k_1^0 r\right). \tag{A 6}$$

For $W > 0$, the fluid velocity near the tube wall is faster than near the axis, while the reverse is true for negative W. Streamlines illustrating the nature of the flow

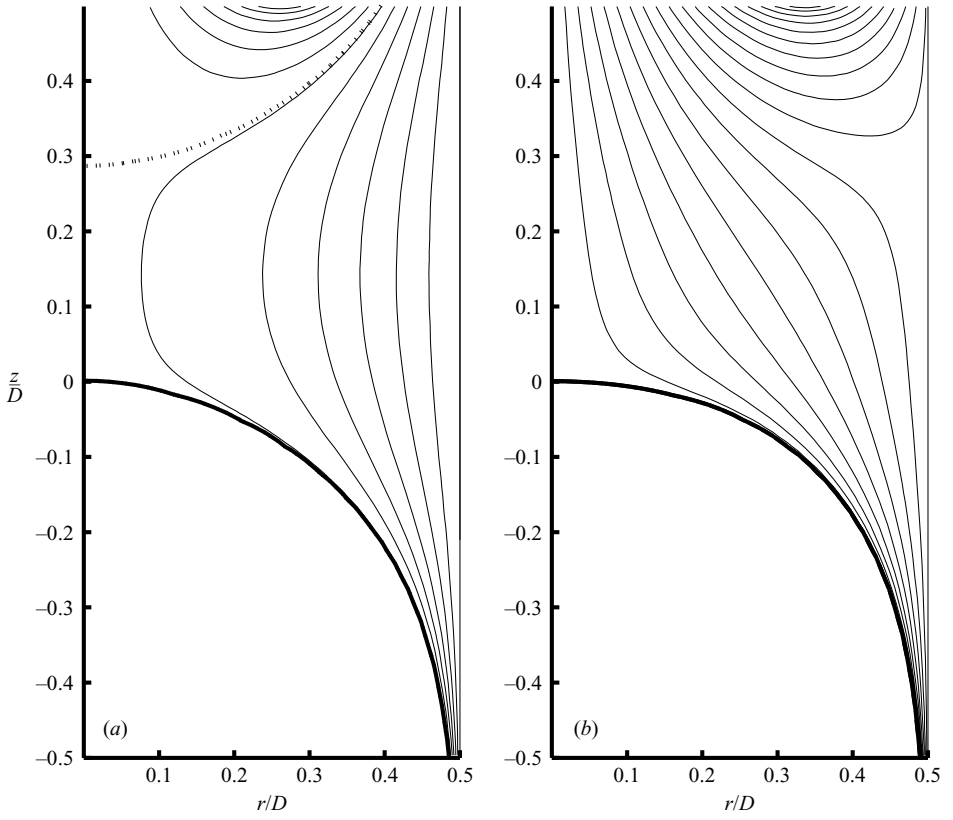

FIGURE 6. Streamlines of the potential base flow of the Appendix for $W = 0.1$ (a) and -0.1 (b). The thick solid line is the bubble surface and the dashed line in (a) the stagnation streamline

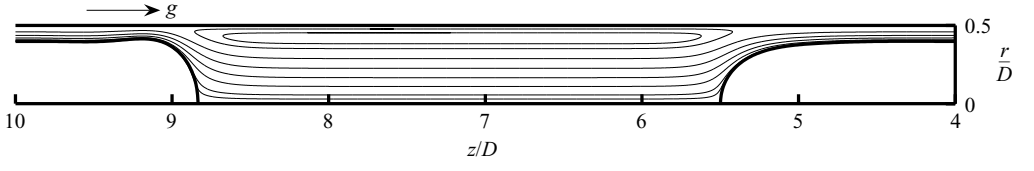

FIGURE 7. Full Navier–Stokes streamlines of the steady axisymmetric flow between two successive bubbles of a periodic bubble train rising against a downward liquid flow with $\overline{U}/\sqrt{gD} = -0.2$. The Morton number is $Mo = g\mu^4/(\rho\sigma^3) = 4.7 \times 10^{-5}$, $Eo = 16.4$, and the spatial period is $L/D = 6$; gravity points to the right and the bubbles move from right to left (from Lu & Prosperetti 2006).

described by (A 1), (A 4) are shown in figure 6 for $W = 0.1$ (a) and $W = -0.1$ (b). Positive values of W result in a stagnation point ahead of the bubble, which approaches the bubble nose as W increases. This flow may mimic the flow behind the closed wake of a preceding bubble. For $W < 0$ the stagnation point moves to the wall. A flow with a similar character is encountered when a periodic bubble train rises against a downward liquid flow as shown in figure 7 (from Lu & Prosperetti 2006). However, the fact that the volumetric flow rate associated with the stream function (A 4) vanishes makes these identifications somewhat artificial as it would imply a vanishing relative velocity between the bubble and the liquid.

The bubble surface is given by $\Psi = 0$ as before:

$$(W - 2U_B)\exp\left(-2k_1^0 Z\right) - W\exp\left(2k_1^0 Z\right) = \frac{2k_1^0 r U_B}{J_0'\left(2k_1^0 r\right)} \tag{A 7}$$

and is also shown in figure 6 by the thick solid lines. The radius of curvature at the nose increases as W is decreased. In this sense, W behaves here as $\overline{U}$ in the flow studied earlier. In order for the bubble to extend in the downstream direction, it is necessary that $U_B - W > 0$.

As before, the bubble rise velocity can be obtained from (2.6) evaluated at an arbitrarily chosen value of r. Upon taking $r = 0$ we find

$$(U_B - W)^3 = \frac{U_B}{2k_1^0}. \tag{A 8}$$

The physical branch of solutions of this equation is the one corresponding to the Davies–Taylor solution for $W = 0$. This branch disappears for $W = -\frac{2}{3}\sqrt{1/(6k_1^0)} \simeq -0.138$, which corresponds to $U_B = \frac{1}{3}\sqrt{1/(6k_1^0)} \simeq 0.0695$. Since the mean liquid velocity in the laboratory frame vanishes, the relative velocity between the bubble and the mean flow is always U_B. Thus, the cases of a stationary and downward moving bubble are not contained in this flow.

A.2. *Perturbation*

For the perturbation, the kinematic boundary condition keeps the same form as (4.5). The dynamic condition is also the same as (4.4) except for the integral term which now vanishes as $\boldsymbol{\Omega} = 0$.

Near the bubble nose $r = 0$, (4.4) and (4.5) become

$$\sum_{j=1}^{N} \dot{\alpha}_j \left(k_j^m\right)^m + (U_B - W)k_1^0 m \sum_{j=1}^{N} \alpha_j \left(k_j^m\right)^m + \left((U_B - W)k_1^0\right)^2 \sum_{j=1}^{N} \beta_j \left(k_j^m\right)^m = 0, \tag{A 9}$$

$$\sum_{j=1}^{N} \dot{\beta}_j \left(k_j^m\right)^m + (U_B - W)k_1^0 (m+2) \sum_{j=1}^{N} \beta_j \left(k_j^m\right)^m - \sum_{j=1}^{N} \alpha_j \left(k_j^m\right)^m \left[m - 4\frac{k_j^m}{k_1^0}(U_B - W)\right] = 0, \tag{A 10}$$

Upon keeping only one term, the result is

$$\dot{\alpha}_1 + (U_B - W)k_1^0 m\alpha_1 + ((U_B - W)k_1^0)^2 \beta_1 = 0, \tag{A 11}$$

$$\dot{\beta}_1 + (U_B - W)k_1^0 (m+2)\beta_1 - \alpha_1 \left[m - 4\frac{k_1^m}{k_1^0}(U_B - W)\right] = 0, \tag{A 12}$$

from which

$$\lambda = (U_B - W)k_1^0 \left[-(m+1) \pm \sqrt{1 - m + 4\frac{k_1^m}{k_1^0}(U_B - W)}\right], \tag{A 13}$$

The corresponding stability condition is

$$U_B - W \leqslant \frac{k_1^0}{4k_1^m} m(m+3) \tag{A 14}$$

which gives $W = -0.131$ for $m = 1$; all other modes are found to be stable. A graph of the maximum eigenvalue vs. W for this calculation is shown in figure 8(a).

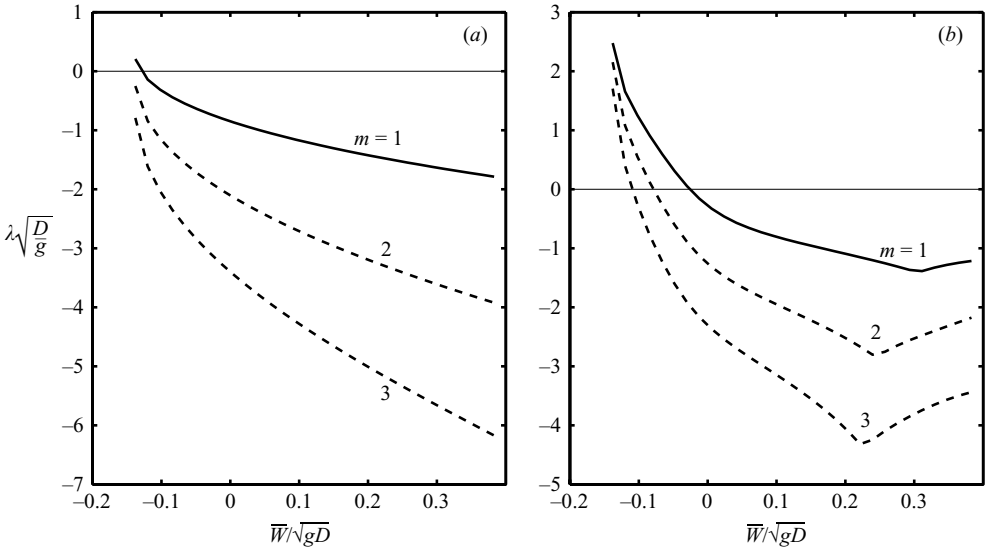

FIGURE 8. (*a*) The largest eigenvalue for the potential base flow of the Appendix as calculated from the near-nose relation (5.3) vs. the parameter W for $m = 1$, 2, and 3. The mode $m = 1$ is unstable for $W < -0.131$. (*b*) The largest eigenvalue for the potential base flow of the Appendix as calculated from (4.4) and (4.5) evaluated at 5 equispaced points between $r = 0$ and $r/D = 0.35$ vs. the parameter W for $m = 1$, 2, and 3. The modes $m = 1$, 2, and 3 are unstable for $W < -0.025$, -0.079, and -0.110, respectively

In order to obtain a more accurate result we evaluate (4.4) and (4.5) at five equispaced points between $r = 0$ and $r = 0.35$ as before. The real part of the dominant eigenvalue for $m = 1$ is shown in figure 8(b). The stability thresholds are found to be $W = -0.025$, -0.079, -0.110 for $m = 1, 2$, and 3, respectively. The apparent break in the slope of the curves is due to the eigenvalue becoming complex.

The flattening of the bubble shape with decreasing W indicates that the mechanism of this instability is similar to the one studied before. In particular, the degree of stretching near the bubble nose, calculated as in § 7, is

$$\left.\frac{\partial U_r}{\partial r}\right|_{0,0} = k_1^0(U_B - W) = \left[\tfrac{1}{2}\left(k_1^0\right)^2 U_B\right]^{1/3} \simeq 1.94 U_B^{1/3}. \tag{A 15}$$

Since U_B is an increasing function of W, again we have a destabilizing effect when W becomes negative. It should be noted that this result is only dependent on the profile of the incident velocity near the bubble nose, as there is no net flow in the tube.

REFERENCES

ABARZHI, S. I. 1998 Stable steady flows in Rayleigh-Taylor instability. *Phys. Rev. Lett.* **81**, 337–340.

BARNEA, D., SHOHAM, O. & TAITEL, Y. 1982 Flow pattern transitions for downward inclined two-phase flow, horizontal to vertical. *Chem. Engng Sci.* **37**, 735–744.

BATCHELOR, G. K. 1987 The stability of a large gas bubble rising through liquid. *J. Fluid Mech.* **184**, 399–422.

BAUMBACH, V., HOPFINGER, E. J. & CARTELLIER, A. 2005 The transient behaviour of a large bubble in a vertical tube. *J. Fluid Mech.* **524**, 131–142.

BENDIKSEN, K. 1984 An experimental investigation of the motion of long bubbles in inclined tubes. *Intl J. Multiphase Flow* **10**, 467–483.

Bendiksen, K. 1985 On the motion of long bubbles in vertical tubes. *Intl J. Multiphase Flow* **11**, 797–812.

Bensimon, D., Pelce, P. & Shraiman, B. I. 1987 Dynamics of curved fronts and pattern selection. *J. Phys. Paris* **48**, 2081–2087.

Vanden Broeck, J.-M. 1984*a* Bubbles rising in a tube and jets falling from a nozzle. *Phys. Fluids* **27**, 1090–1093.

Vanden Broeck, J.-M. 1984*b* Rising bubble in a two-dimensional tube with surface tension. *Phys. Fluids* **27**, 2604–2607.

Vanden Broeck, J.-M. 1991 Axisymmetric jet falling from a vertical nozzle and bubble rising in a tube of circular cross section. *Phys. Fluids* A **3**, 258–262.

Clanet, C., Héraud, P. & Searby, G. 2004 On the motion of bubbles in vertical tubes of arbitrary cross section: some complements to the Dumitrescu-Taylor problem. *J. Fluid Mech.* **519**, 359–376.

Collins, R., De Moraes, F., Davidson, J. & Harrison, D. 1978 The motion of a large gas bubble rising through liquid flowing in a tube. *J. Fluid Mech.* **89**, 497–514.

Davies, R. & Taylor, G. 1950 The mechanics of large bubbles rising through extended liquids and through liquids in tubes. *Proc. R. Soc. Lond.* A **200**, 375–390.

Dumitrescu, D. T. 1943 Strömung an einer luftblase in senkrechten rohr. *Z. Angew. Math. Mech.* **23**, 139–149.

Epstein, R. 2004 On the Bell-Plesset effects: The effects of uniform compression and geometrical convergence on the classical Rayleigh-Taylor instability. *Phys. Plasmas* **11**, 5114–5124.

Fabre, J. & Liné, A. 1992 Modeling of two-phase slug flow. *Annu. Rev. Fluid Mech.* **24**, 21–46.

Frankel, I. & Weihs, D. 1987 Influence of viscosity on the capillary instability of a stretching jet. *J. Fluid Mech.* **185**, 361–383.

Funada, T., Joseph, D. D., Maehara, T. & Yamashita, S. 2005 Ellipsoidal model of the rise of a Taylor bubble in a round tube. *Intl J. Multiphase Flow* **31**, 473–491.

Garabedian, P. R. 1957 On steady-state bubbles generated by Taylor instability. *Proc. R. Soc. Lond.* A **241**, 423–431.

Griffith, P. & Wallis, G. 1961 Two-phase slug flow. *J. Heat Transfer* **83**, 307–320.

Ha-Ngoc, H. & Fabre, J. 2004 Test-case No. 29B: The velocity and shape of 2D long bubbles in inclined channels or in vertical tubes (PA, PN) Part II: In a flowing liquid. *Multiphase Sci. Technol.* **16**, 191–206.

Hartunian, R. A. & Sears, W. R. 1957 On the stability of small gas bubbles moving uniformly in various liquids. *J. Fluid Mech.* **3**, 27–47.

Kawanishi, K., Hirao, Y. & Tsuge, A. 1990 An experimental study on drift flux parameters for two-phase flow in vertical round tubes. *Nucl. Engng Des.* **120**, 447–458.

Lamb, H. 1932 *Hydrodynamics*, 6th edn. Cambridge University Press.

Layzer, D. 1955 On the instability of superposed fluids in a gravitational field. *Astrophys. J.* **122**, 1–12.

Levine, H. & Yang, Y. 1990 A rising bubble in a tube. *Phys. Fluids* A **2**, 542–546.

Lu, X. & Prosperetti, A. 2006 A numerical study of laminar slug flow. *Intl J. Multiphase Flow*, submitted.

Martin, C. S. 1976 Vertically downward two-phase slug flow. *Trans. ASME: J. Fluids Engng* **98**, 715–722.

Meiron, D. I. 1989 On the stability of gas bubbles rising in an inviscid fluid. *J. Fluid Mech.* **198**, 101–114.

Mukherjee, H. & Brill, J. P. 1985 Empirical equations to predict flow patterns in two-phase inclined flow. *Intl J. Multiphase Flow* **11**, 299–315.

Nickens, H. & Yannitel, D. 1987 The effect of surface tension and viscosity on the rise velocity of a large gas bubble in a closed vertical liquid-filled tube. *Intl J. Multiphase Flow* **13**, 57–69.

Nicklin, D. J. 1962 Two-phase bubbly flow. *Chem. Engng Sci.* **17**, 693–702.

Nicklin, D., Wilkes, J. & Davidson, J. 1962 Two-phase flow in vertical tubes. *Trans. Inst. Chem. Engrs* **40**, 61–68.

Nie, Q. & Tanveer, S. 1995 The stability of a two-dimensional rising bubble. *Phys. Fluids* **7**, 1292–1306.

Nigmatulin, T. R. 2001 Surface of a Taylor bubble in vertical cylindrical flows. *Dokl. Phys.* **46**, 803–805.

Plesset, M. S. 1954 On the stability of fluid flows with spherical symmetry. *J. Appl. Phys.* **25**, 96–98.

Plesset, M. S. & Prosperetti, A. 1977 Bubble dynamics and cavitation. *Annu. Rev. Fluid Mech.* **9**, 145–185.

Polonsky, S., Shemer, L. & Barnea, D. 1999 The relation between the Taylor bubble motion and the velocity field ahead of it. *Intl J. Multiphase Flow* **25**, 957–975.

Saffman, P. G. 1986 Viscous fingering in Hele-Shaw cells. *J. Fluid Mech.* **173**, 73–94.

Spedding, P. & Nguyen, V. 1980 Regime maps for air water two phase flow. *Chem. Engng Sci.* **35**, 779–793.

Tanveer, S. 1987 Analytic theory for the linear stability of the Saffman-Taylor finger. *Phys. Fluids* **30**, 2318–2329.

Taylor, G. I. & Saffman, P. G. 1959 A note on the motion of bubbles in a Hele-Shaw cell and porous medium. *Q. J. Mech. Appl. Maths* **12**, 265–279.

Tung, K. W. & Parlange, J. Y. 1976 Note on the motion of long bubbles in closed tubes – Influence of surface tension. *Acta Mechanica* **24**, 313–317.

Viana, F., Pardo, R., Yánez, R., Trallero, J. L. & Joseph, D. D. 2003 Universal correlation for the rise velocity of long gas bubbles in round pipes. *J. Fluid Mech.* **494**, 379–398.

White, E. T. & Beardmore, R. H. 1962 The velocity of rise of single cylindrical air bubbles through liquids contained in vertical tubes. *Chem. Engng Sci.* **17**, 351–361.

Zel'dovich, Ya. B., Istratov, A. G., Kidin, N. I. & Librovich, V. B. 1980 Flame propagation in tubes: hydrodynamics and stability. *Combust. Sci. Tech.* **24**, 1–13.

Zukoski, E. 1966 Influence of viscosity, surface tension, and inclination angle on motion of long bubbles in closed tubes. *J. Fluid Mech.* **25**, 821–837.